Helically corrugated waveguide with dielectric lined drift section for a 263 GHz gyro-TWT

Max Vöhringer[#$], Alexander Marek[*], Stefan Illy[#], Manfred Thumm[#$], Lukas Feuerstein[#], Chuanren Wu[#], John Jelonnek[#$]

[#]IHM, Karlsruhe Institute of Technology (KIT), Germany
[$]IHE, Karlsruhe Institute of Technology (KIT), Germany
[*]Fraunhofer-Institute for High-Frequency Physics and Radar Techniques (FHR), Germany
max.voehringer@kit.edu

***Abstract* — Gyro-TWTs with helically corrugated interaction region (HCIR) have shown to be effective for broadband and high-power amplification of signals up to the W-band. In this publication, versions for 263 GHz (G-band) are proposed, which are able to generate above 1 kW of output power with a gain of 30 dB and 50 dB respectively. To avoid self-oscillations, a dielectric lined drift section is introduced and its effect on the interaction investigated. Furthermore, the effect of a non-ideal electron beam on the amplifier gain is examined. It is found that it has a great influence on the bandwidth; its influence on the maximum gain, however, is limited.**

***Keywords* — gyrotron traveling wave amplifier, broadband amplification, helically corrugated waveguide.**

I. Introduction

Dynamic Nuclear Polarization (DNP) has been shown to be a very effective technique to enhance Nuclear Magnetic Resonance (NMR) performance. It uses the electron magnetic moment, which is approximately 660 times larger than that of the proton [1], used in ordinary NMR. By coupling the nuclei to the more strongly polarized electrons, the DNP-NMR technique increases the nuclear spin polarization by two to five orders of magnitude and thus reduces the necessary acquisition time in experiments by a factor of up to 10^4 [2].

The key for DNP-NMR is the strong irradiation of the NMR sample by high-power microwaves in the sub-THz range. Assuming commercially available systems starting from an NMR frequency at 400 MHz, the corresponding microwave sources must operate in the sub-THz frequency range, at 263 GHz and above. Today, commercially available DNP-NMR systems are considering a field-dependent, continuous wave (CW) approach to transfer the polarization from electrons to other nuclei. However, coherent, pulsed polarization transfer [3] offers a significant potential for a more efficient polarization transfer, which can ultimately increase the rate at which the nuclear spins may be polarized, as well as the maximum polarization. Pulsed DNP sequences, as for example, NOVEL [4] and TOP DNP [2] at high magnetic fields, are part of current research and high-power microwave pulses up to 1 kW at 263 GHz are desired.

To generate coherent microwave pulses of sufficient power, high-power amplifiers are required. Promising amplifier concepts are the dielectric-loaded gyro-TWT [5] and the so-called helical gyro-TWT [6]. The first suppresses self-oscillations originating from internal feedback by introducing lossy elements inside the interaction circuit [7]. The second improves bandwidth and reduces susceptibility towards velocity spreads in the electron beam by utilizing helical corrugations along the interaction circuit, the so-called helically corrugated interaction region (HCIR). Furthermore, this approach brings the advantage of operating at the second harmonic, which reduces the required static magnetic field by a factor of 2. This is especially important when operating at higher frequencies; in this case, the static magnetic field decreases from 10 T to 5 T. This enables the use of NbTi superconductor, which is simpler to produce and therefore more affordable than Nb_3Sn superconductors generally used for 10 T magnets. Because of all these benefits, this publication is focusing on the helical gyro-TWT.

II. Helically Corrugated interaction region

A. Theory

The HCIR consists of a cylindrical shape with corrugations in azimuthal as well as axial direction. The radius r is described by

$$r(\theta, z) = r_0 + r_1 \cos\left(m_\mathrm{B}\theta + \frac{2\pi z}{d}\right) \tag{1}$$

in a cylindrical coordinate system. Here, r_0 denotes the mean radius, r_1 the corrugation amplitude, and d the corrugation period. The number of corrugations along the azimuthal direction is given by m_B; it defines which circular waveguide modes are coupled by the corrugations. The Bragg resonance conditions have to be met. Therefore, the azimuthal indices m_i of the two modes have to fulfil $m_1 + m_2 = m_\mathrm{B}$ and the wavenumber of mode 2 has to be close to $2\pi d$ if mode 1 is close to cut-off [6]. In this work a HCIR with $m_\mathrm{B} = 3$, coupling $TE_{1,1}$ and $TE_{2,1}$ circular waveguide modes, is used, which rotate in opposite directions. Compared to higher m_B it has the benefit of not needing an additional mode converter. The fundamental $TE_{1,1}$ circular waveguide mode can be used at input and output. Also, mode competition is greatly reduced for smaller diameters. A 3D depiction of a $m_\mathrm{B} = 3$ HCIR vacuum region can be seen in Fig. 1.

© 2025 IEEE. Personal use of this material is permitted. Permission from IEEE must be obtained for all other uses, in any current or future media, including reprinting/republishing this material for advertising or promotional purposes, creating new collective works, for resale or redistribution to servers or lists, or reuse of any copyrighted component of this work in other works.

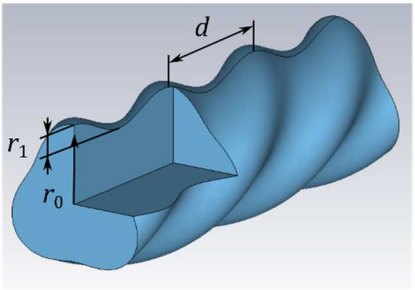

Fig. 1. Vacuum region of a 3-fold HCIR ($m_B = 3$). The Vacuum region is surrounded by copper.

As an electron beam, an axis encircling beam or large orbit beam is used. It is created by electrons passing through a cusp in a static magnetic field [8]. The electron beam transfers energy to the RF-wave when the resonant condition [9]

$$\omega \approx s\omega_c + k_z v_z \qquad (2)$$

is fulfilled. Here, ω denotes the angular frequency of the RF-wave, ω_c the electron resonant frequency, s the harmonic number, k_z the axial wavenumber and v_z the axial electron velocity.

B. Optimization for 263 GHz

The gyro-TWT is designed to work around the desired center frequency of 263 GHz, therefore the HCIR must be optimized for the same frequency. As a first step, the phase difference between an electron, with known parameters and unaffected by any RF-wave and the RF-wave E-field vector at the end of the interaction region shall be calculated. Therefore, the dispersion properties of the HCIR need to be known. This is achieved by performing a coordinate transformation to unwind the HCIR to get rid of its z-dependency. The problem is therefore reduced from 3D to 2D. After that, a 2D Vector Finite-Element Method [10] is then utilized to get the dispersion of its eigenmodes. The dispersion as well as the electron beam line, derived from the right side of equation (2), are plotted in the dispersion diagram, seen in Fig. 2. With the frequency offset, the total length of the HCIR and the required time for an electron to pass through the HCIR, the phase difference at the end of the HCIR can be calculated. It should not be larger than π, so the bunched electrons stay in the deceleration phase and do not enter the acceleration phase, which would lead to over-bunching, where the wave starts transferring energy back to the electron beam. The chosen parameters for the HCIR are then verified via PIC simulations with CST Microwave Studio. At 263 GHz, the determined parameters for the HCIR are $r = 0.544$ mm, $r = 0.08$ mm and $d = 1.16$ mm. For these parameters, an electron beam with an energy of 50 keV, current of 0.6 A, and a pitch factor $\alpha = v_t/v_z$, the ratio between transversal velocity v_t and axial velocity v_z, of 1.0 in a static axial magnetic field of 4.96 T, interacts with the RF-wave.

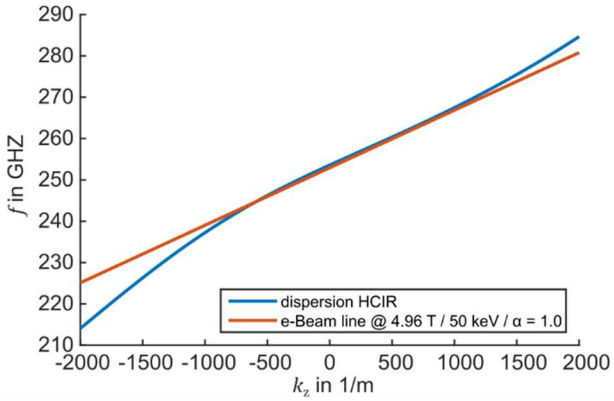

Fig. 2. Dispersion of the HCIR and electron beam line derived from the interaction condition (equation (2)).

For a HCIR with a length of $32d$ the maximum gain of 30 dB is reached. Therefore, a 1 W input signal results in the desired 1 kW output signal. The 3 dB bandwidth is 24.6 GHz, as shown by the blue line in Fig. 3.

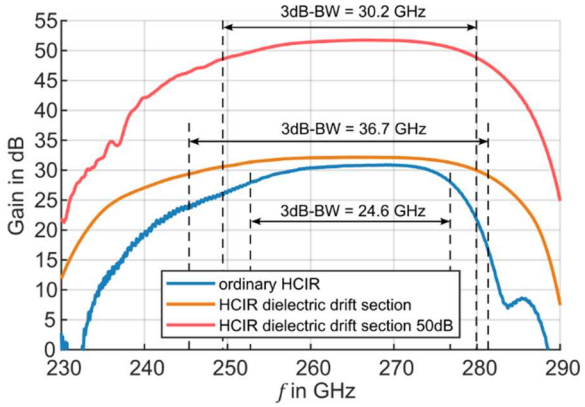

Fig. 3. Frequency dependency of the amplifier gain for three different interaction circuits, the ordinary HCIR as well as HCIRs with dielectric drift regions designed for 30 dB and 50 dB of gain.

C. Effect of reflections at HCIR Input and Output

The before-mentioned results are reached by omitting the imperfections of the components at the input and output of the HCIR. However, the tapers at both ends of the HCIR included in the simulations, if designed correctly they do not influence the HCIR performance. In reality, the components at the two ports can cause certain reflections, described by their S_{11}-Parameters. Given the high frequency and therefore low tolerances, reflections can easily occur. Here, a worst-case scenario is considered where at both ends of the HCIR reflections of -10 dB are occurring. The reflected wave at the output travels back through the amplifier and modulates the electron beam at the input. For the ordinary HCIR this leads to self-oscillation, as seen in Fig. 4.

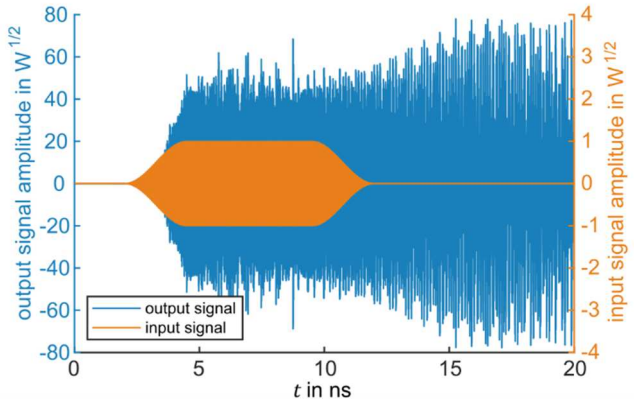

Fig. 4. Input and output signal amplitude for an ordinary HCIR. The input signal has a power of 1 W. Only the power in one polarization is plotted. Due to the fact that the wave inside the HCIR is a circular polarized wave with equal power in both polarization directions only half the total power is considered in this figure

III. HCIR WITH DIELECTRICALLY LINED DRIFT SECTION

A. Working Principle

To solve the problem of self-oscillation encountered in the previous section, the HCIR layout is changed. Instead of one continuous wave traveling through a continuous gain section, the interaction circuit is split into three parts, as depicted in the lower part of Fig. 5. First, the modulating section, where the input signal modulates the electron beam. Second, the drift section, here the electron beam bunches in the absence of any RF-wave, which is attenuated by a lossy dielectric at the walls. Third, the gain section, where the bunched electron beam excites an electromagnetic wave to which it transfers part of its energy.

This is already utilized in W-band gyro-TWTs presented in [11], where a cutoff section is used to keep the drift section RF-wave free, also [12] is using a similar approach. Here the drift section is above cutoff and the wave is absorbed by lossy sections at both of its ends. Given the fact that the diameter of the HCIR for 263 GHz is just over 1 mm, the later approach is chosen to avoid a further reduction in diameter.

The benefit of separating the modulation and gain section is to suppress self-oscillations by introducing losses for the reflected waves, as shown in [12]. Another advantage of this design is that it can be manufactured individually. The manufacturing of the complex helical shape is cut is now only $10d$, which gives an aspect ratio close to 10, not the 32 of the ordinary HCIR.

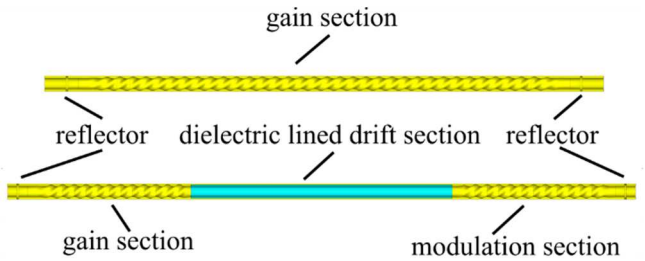

Fig. 5. Ordinary HCIR (top) and HCIR with dielectric lined drift section (bottom).

B. Simulation

As an absorbing material BeO-TiO2, with a dielectric with a real part of 10 and an imaginary part of 4, is used [13]. The thickness is 0.1 mm, here the $TE_{1,1}$-mode experiences the highest attenuation. The length of the dielectric lined section is 26 mm. This approach is able to prevent self-oscillation, as depicted in Fig. 6, where the input signal is amplified without causing any oscillations. Furthermore, bandwidth increases to 36.7 GHz, as depicted in Fig 3 (orange line). One disadvantage is the increased overall length of the HCIR with dielectric lined drift section compared to the ordinary HCIR, as seen in Fig. 5. However, the benefits greatly outweigh the increase in length.

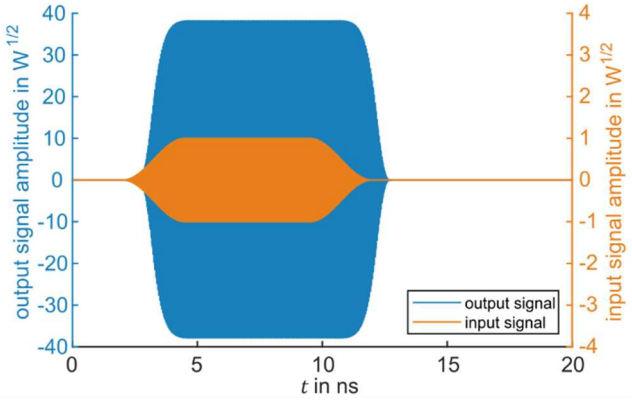

Fig. 6. Input and output signal amplitude for an ordinary HCIR. The input signal has a power of 1 W. Only the power in one polarization is plotted. Due the same reason given in the description of Fig 4.

C. Results

The HCIR with dielectric lined drift section effectively prohibits self-oscillations at 263 GHz. This opens the possibility to develop HCIRs with even higher gains. For that, a high-gain version with 50 dB gain is designed by increasing the length of the drift section to 42 mm. This enables a much-reduced input power of 10 mW to gain the same desired 1 kW output power, as shown in Fig. 3 (red line). Even with the higher gain, no self-oscillation occurs, as shown in Fig. 7.

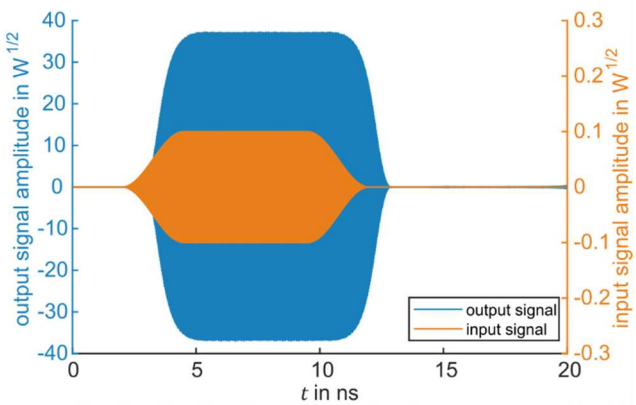

Fig. 7. Input and output signal amplitude for an ordinary HCIR. The input signal has a power of 10 mW. Only the power in one polarization is plotted. Due the same reason given in the description of Fig 4.

IV. Influence of Electron Beam Velocity Spreads

Until now, the electron beam was considered ideal for all the simulations. This means every electron has the same energy as well as pitch factor α. In reality, this will not be the case, due to the surface roughness of the emitter as well as other imperfections of the electron gun. The velocity spreads are described as a standard deviation $\delta\alpha$.

The influence of the imperfect electron beam on the gain of the HCIR with a dielectric lined drift section, including input and output reflections is investigated. Therefore, interaction simulations are conducted with electron beams of different standard deviations $\delta\alpha$ and the results are depicted in Fig. 8. It is obvious that for lower $\delta\alpha$ the influence is not too severe. However, if $\delta\alpha$ is 10 % or larger, the bandwidth contracts quite significantly, especially for the higher frequencies, which leads to a shift in the center frequency. It is therefore critical to have a high-quality electron beam from a CUSP-type electron gun like in [14]. However, even for a well-performing electron gun, the electron beam is estimated to have a $\delta\alpha$ of 10-15 % at 263 GHz including all imperfections of the electron emitter, even if a well-designed electron gun is used. In this case, the bandwidth is reduced to 14.7 GHz for a $\delta\alpha$ of 15 %. This constitutes a large decline in bandwidth, but is still enough for DNP-NMR experiments. The maximum gain does not reduce significantly. Therefore, the desired output power can be reached even with non-ideal electron beam.

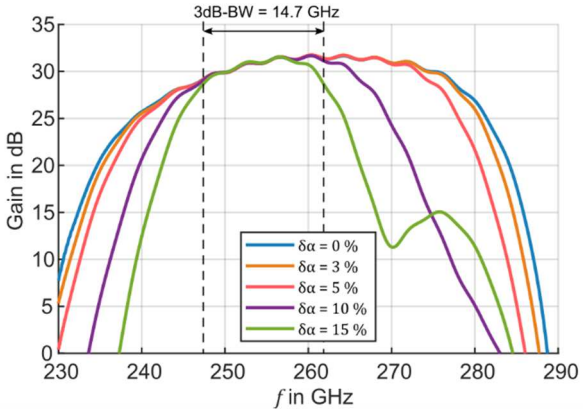

Fig. 8. Frequency dependency of the amplifier gain for non-ideal electron beams with different pitch factor standard deviations $\delta\alpha$.

V. Conclusion

In this publication, an ordinary HCIR with 30 dB of gain is proposed to amplify a 1 W input signal to a 1 kW output signal. However, it suffers from self-oscillation when non-ideal input and output reflections of -10 dB are considered. This could be remedied by introducing a dielectric lined drift section into the HCIR. With this approach it is also possible to go beyond a gain of 30 dB and a 50 dB version is introduced. It is able to operate without self-oscillation, even if high reflections of -10 dB at its ports are considered. Furthermore, the influence of a non-ideal electron beam is investigated, which shows a significant reduction in the bandwidth, especially for higher pitch factor spreads, compared to the ideal electron beam. However, the bandwidth is still sufficient for the intended use case. On the other hand, the maximum gain is not impeded by decreasing beam quality, which ensures an output power of up to 1 kW is still reached, even with decreasing beam quality.

Acknowledgment

The results presented here have been obtained within the frame of the CRC 1527 “HyPERiON” supported by German Research Association DFG (Deutsche Forschungsgesellschaft SFB 1527).

References

[1] A. J. Rossini, A. Zagdoun, M. Lelli, A. Lesage, C. Copéret, and L. Emsley, “Dynamic Nuclear Polarization Surface Enhanced NMR Spectroscopy,” Accounts of Chemical Research, vol. 46, no. 9, pp. 1942–1951, Sep. 17, 2013. DOI: 10.1021/ar300322x.

[2] K. O. Tan, M. Mardini, C. Yang, J. H. Ardenkjær-Larsen, and R. G. Griffin, “Three-spin solid effect and the spin diffusion barrier in amorphous solids,” Science Advances, vol. 5, no. 7, eaax2743, Jul. 26, 2019. DOI: 10.1126/sciadv.aax2743. (2023).

[3] G. Mathies, S. Jain, M. Reese, and R. G. Griffin, “Pulsed Dynamic Nuclear Polarization with Trityl Radicals,” The Journal of Physical Chemistry Letters, vol. 7, no. 1, pp. 111–116, Jan. 7, 2016. DOI: 10.1021/acs.jpclett.5b02720.

[4] T. V. Can, J. J. Walish, T. M. Swager, and R. G. Griffin, “Time domain DNP with the NOVEL sequence,” The Journal of Chemical Physics, vol. 143, no. 5, p. 054 201, Aug. 7, 2015. DOI: 10.1063/1.4927087

[5] W. Jiang *et al.*, “Experimental Demonstration of a 10-kW-Level G-Band Gyro-TWT,” *IEEE Electron Device Lett.*, vol. 45, no. 5, pp. 905–908, May 2024, doi: 10.1109/LED.2024.3375857.

[6] G. G. Denisov, V. L. Bratman, A. D. R. Phelps, and S. V. Samsonov, “Gyro-TWT with a helical operating waveguide: new possibilities to enhance efficiency and frequency bandwidth,” *IEEE Trans. Plasma Sci.*, vol. 26, no. 3, pp. 508–518, Jun. 1998, doi: 10.1109/27.700785.

[7] L. R. Barnett, J. M. Baird, Y. Y. Lau, K. R. Chu, and V. L. Granatstein, “A high gain single stage gyrotron traveling-wave amplifier,” in *1980 International Electron Devices Meeting*, IRE, 1980, pp. 314–317. doi: 10.1109/IEDM.1980.189823.

[8] K. Shinano and H. Itô, “Behavior of a Charged Particle in a Cusp Field,” *J. Phys. Soc. Jpn.*, vol. 21, no. 9, pp. 1822–1829, Sep. 1966, doi: 10.1143/JPSJ.21.1822.

[9] S. J. Cooke and G. G. Denisov, “Linear theory of a wide-band gyro-TWT amplifier using spiral waveguide,” *IEEE Trans. Plasma Sci.*, vol. 26, no. 3, pp. 519–530, Jun. 1998, doi: 10.1109/27.700786.

[10] S. V. Mishakin and S. V. Samsonov, “Analysis of Dispersion and Losses in Helically Corrugated Metallic Waveguides by 2-D Vector Finite-Element Method,” *IEEE Transactions on Microwave Theory and Techniques*, vol. 59, no. 9, pp. 2189–2196, Sep. 2011, doi: 10.1109/TMTT.2011.2160201.

[11] S. V. Samsonov, A. A. Bogdashov, G. G. Denisov, I. G. Gachev, and S. V. Mishakin, “Cascade of Two W -Band Helical-Waveguide Gyro-TWTs With High Gain and Output Power: Concept and Modeling,” *IEEE Trans. Electron Devices*, vol. 64, no. 3, pp. 1305–1309, Mar. 2017, doi: 10.1109/TED.2016.2646065.

[12] C. R. Donaldson, P. MacInnes, C. W. Robertson, L. Zhang, and C. G. Whyte, “Investigations of a high gain W-band gyro-TWA,” in *2021 46th International Conference on Infrared, Millimeter and Terahertz Waves (IRMMW-THz)*, Aug. 2021, pp. 1–2. doi: 10.1109/IRMMW-THz50926.2021.9567290.

[13] C. Lu *et al.*, “Design and Power Capacity Investigation of a Q-Band 100-kW-Continuous-Wave Gyro-TWT,” *IEEE Trans. Electron Devices*, vol. 71, no. 3, pp. 2126–2132, Mar. 2024, doi: 10.1109/TED.2024.3354684.

[14] M. Vöhringer *et al.*, “Universal CUSP-Type Electron Gun for Helical Gyro-TWTs for DNP-NMR Applications,” in *2023 48th International Conference on Infrared, Millimeter, and Terahertz Waves (IRMMW-THz)*, Montreal, QC, Canada: IEEE, Sep. 2023, pp. 1–2. doi: 10.1109/IRMMW-THz57677.2023.10299143.